Front. Earth Sci. 2024, 18(1): 30–43
https://doi.org/10.1007/s11707-022-1011-4

RESEARCH ARTICLE

Fine classification of rice paddy using multitemporal compact polarimetric SAR C band data based on machine learning methods

Xianyu GUO[1], Junjun YIN[1], Kun LI[2], Jian YANG[3], Huimin ZOU[4], Fukun YANG (✉)[4]

1 School of Computer and Communication Engineering, University of Science and Technology Beijing, Beijing 100083, China
2 Aerospace Information Research Institute, Chinese Academy of Sciences, Beijing 100094, China
3 Department of Electronic Engineering, Tsinghua University, Beijing 100084, China
4 College of Global Change and Earth System Science, Beijing Normal University, Beijing 100875, China

Abstract Rice is an important food crop for human beings. Accurately distinguishing different varieties and sowing methods of rice on a large scale can provide more accurate information for rice growth monitoring, yield estimation, and phenological monitoring, which has significance for the development of modern agriculture. Compact polarimetric (CP) synthetic aperture radar (SAR) provides multichannel information and shows great potential for rice monitoring and mapping. Currently, the use of machine learning methods to build classification models is a controversial topic. In this paper, the advantages of CP SAR data, the powerful learning ability of machine learning, and the important factors of the rice growth cycle were taken into account to achieve high-precision and fine classification of rice paddies. First, CP SAR data were simulated by using the seven temporal RADARSAT-2 C-band data sets. Second, 20-two CP SAR parameters were extracted from each of the seven temporal CP SAR data sets. In addition, we fully considered the change degree of CP SAR parameters on a time scale (ΔCP_{DoY}). Six machine learning methods were employed to carry out the fine classification of rice paddies. The results show that the classification methods of machine learning based on multitemporal CP SAR data can obtain better results in the fine classification of rice paddies by considering the parameters of ΔCP_{DoY}. The overall accuracy is greater than 95.05%, and the Kappa coefficient is greater than 0.937. Among them, the random forest (RF) and support vector machine (SVM) achieve the best results, with an overall accuracy reaching 97.32% and 97.37%, respectively, and Kappa coefficient values reaching 0.965 and 0.966, respectively. For the two types of rice paddies, the average accuracy of the transplant hybrid (T-H) rice paddy is greater than 90.64%, and the highest accuracy is 95.95%. The average accuracy of direct-sown japonica (D-J) rice paddy is greater than 92.57%, and the highest accuracy is 96.13%.

Keywords compact polarimetric (CP) SAR, rice paddy, machine learning, fine classification, multitemporal

1 Introduction

Rice is the second most important agricultural plant in the world, after wheat, in terms of cultivated area and total production. The accurate classification of paddy fields is critical in agricultural monitoring and management, pre-estimation of the expected rice yields, and prevention and control of diseases and insect pests. Recently, with an increase in the amount of remote sensing data, the demand for large-scale, fine rice paddy classification has grown and attracted the interest of many researchers. However, traditional, optical remote sensing data are easily affected by cloudy and rainy weather in rice planting areas, so they expose the limited capacity of the fine classification of rice paddies. Synthetic aperture radar (SAR) has become a powerful tool and an indispensable means of the fine classification of rice paddies because of its ability to operate at all times and under all weather conditions (Le Toan et al., 1997; Shao et al., 2001; Bouvet et al., 2009).

Currently, there are four types of methods for rice paddy mapping using SAR data. First, the time-changing rule based on rice backscattering characteristics is considered (Le Toan et al., 1989, 1997; Kurosu et al., 1995; Bouvet et al., 2009; Inoue and Sakaiya 2013). Second,

Received November 16, 2022; accepted May 9, 2023

E-mail: yangfk@radi.ac.cn

certain researchers use backscattering coefficients of rice with different polarizations (Chen and Li 2008; Bouvet et al., 2009). The above two methods are based on multitemporal single/multipolarization SAR data and only use backscattering intensity information, without the phase information of radar echo (Yang et al., 2014). The third method is mainly based on the scattering mechanism of rice. Advanced methods of polarization SAR data processing, such as polarization decomposition, are utilized to analyze the scattering mechanism of rice and to distinguish rice and other nonrice classes based on the large contribution of double-bounce scattering of rice (Li et al., 2011 and 2012a). Fourth, with the rapid development of machine learning methods in recent years, certain researchers have applied the random forest (RF) (Waske and Braun 2009; van Beijma et al., 2014; Yu et al., 2018; Zhang et al., 2021), support vector machine (SVM) (Lardeux et al., 2009, 2011; Betbeder et al., 2013; Dusseux et al., 2014; Abubakar et al., 2020; Gasparovic and Dobrinic, 2021) and other machine learning methods (de Castro Filho et al., 2020) to large-scale and rapid research on crop mapping, in particular, the classification of rice and nonrice classes (Kucuk et al., 2016; Ndikumana et al., 2018; Onojeghuo et al., 2018; Park et al., 2018; Ranjan and Parida, 2019; Thorp and Drajat, 2021).

Although full-polarization SAR has great advantages in rice paddy mapping, its pulse repetition frequency is twice that of single-polarization and dual-polarization systems, and its pulse width is relatively small, which limits its application in large-scale rice paddy mapping. However, the CP SAR system cannot only reduce the complexity and energy consumption of sensors but also provide relatively abundant polarization information and a larger width. Therefore, CP SAR data are one of the best choices for rice paddy mapping under the conditions of both mapping accuracy and mapping area. In 2013, Brisco et al. (2013) completed rice paddy mapping based on CP SAR simulation data and compared and analyzed the mapping accuracy of single-polarization, compact-polarization, and full-polarization SAR data. The results showed the good performance of CP SAR data in rice paddy mapping, which was comparable to that of full-polarization data and far superior to that of single-polarization and double-polarization SAR data. In 2014, Yang et al. (2014) built a decision tree (DT) algorithm by analyzing rice scattering characteristics using multitemporal CP SAR data and achieved good rice paddy mapping results. In 2015, Uppala et al. identified rice crops by using single date hybrid polarimetric data available from RISAT-1 SAR (Uppala et al., 2015). Guo et al. (2018) obtained high-precision classification results of rice paddies based on the feature selection method and SVM and DT classification algorithms by using multitemporal CP SAR data. In summary, Brisco and Uppala's studies showed that CP SAR data had great application potential in rice paddy mapping. However, these studies only classified rice and nonrice classes and did not address the classification of different varieties and sowing methods of rice. In addition, Yang's and Guo's studies require much time to analyze the CP SAR parameters of rice and to establish a suitable DT, which leads to low timeliness of results application. Therefore, the problem of fast and high-efficiency, fine classification of rice paddies based on CP SAR data is still an urgent research focus and challenge. However, in recent years, with an increase in the prosperity of machine learning methods, the use of machine learning methods to achieve the fine classification of rice paddies with CP SAR data has become a possibility.

Therefore, the present study fully considers the advantages of CP SAR data, the powerful learning and rapid problem-solving abilities of machine learning, and the important factors of the rice growth cycle. First, seven temporal CP SAR images were obtained, and then 20-two CP SAR parameters and ΔCP_{DoY} were extracted for each temporal SAR data. Second, six machine learning methods were utilized for the fine classification of rice paddies. Last, six classification results were compared, verified, and discussed.

2 Study area and data sources

The study area of this paper is the junction area of Hongze and Xuyi, Jiangsu, China. This junction is

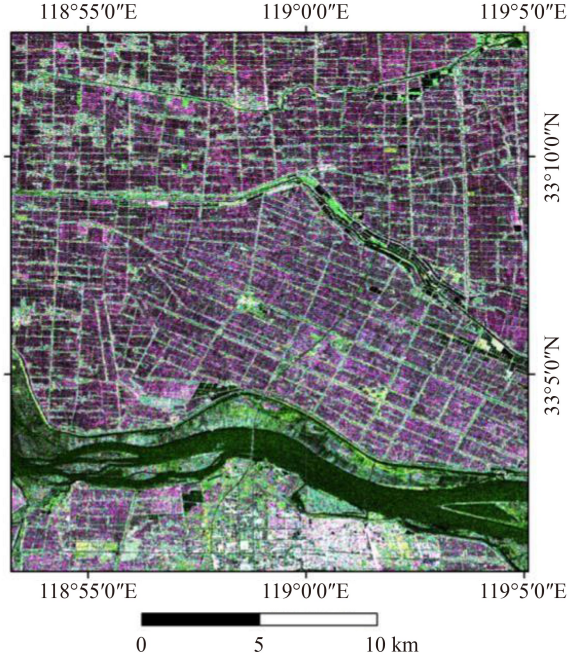

Fig. 1 Color composite images (CP SAR RR (red), RV (green), RH (blue)) of the backscattering coefficients of simulated CP SAR data in the study area on August 28, 2012.

located between 118°41′34″E–119°16′27″E and 33°17′05″N–33°56′39″N, which is a major production area of rice in eastern China. The study area is approximately 40 km × 30 km, which mainly comprises a lakeside plain, with a ground height between 5 and 9 m (Fig.1). The area experiences a subtropical warm monsoon climate, with an annual rainfall of approximately 1085 mm and abundant annual sunshine in four distinct seasons. This region's farmland is regular with a larger planting scale. Moreover, the rice at the test site is ripe once a year, and its growing season is from mid-June to late October. The main rice species in this study area are hybrid and japonica, and the sowing method is transplanting or direct sowing. In this study, the fine classification of rice paddy fields was mainly investigated for two types: rice transplanting indica paddy fields (T-H) and direct-sown japonica (D-J) paddy fields. Figure 2 shows an image of the seven phenological periods of rice growth for the T-H rice paddy in the study area.

The data sets as the basic data source of this paper consisted of seven temporal RADARSAT-2 full-polarization SAR single-looking complex (SLC) data sets with a central frequency of 5.405 GHz (C-band) and an orbital direction of the ascending orbit. The specific parameters of the multitemporal RADARSAT-2 data sets are shown in Table 1. Seven temporal RADARSAT-2 full-polarization SAR data sets were selected to simulate CP SAR data. The simulated CP SAR data exhibited circular polarization transmitting and linear polarization receiving mode (transmitting right circular polarization, receiving horizontal polarization and vertical polarization) (Raney et al., 2012a), with a resolution of 30 m and a noise level of −25 dB. Figure 1 shows the color composite (red–green-blue) images of the backscattering coefficients of simulated CP SAR data in the study area on August 28, 2012.

During the passage of the RADARSAT-2 satellite, field synchronization work was carried out, and the position, area, and boundary of 30-five rice sample parcels were recorded with a high-precision global positioning system (GPS), including 24 T-H plots and 11 D-J plots. The position, area, and boundary of eight water areas, eight shoal areas, and ten urban areas were also selected and recorded, except for the rice sample. A total of 56266 samples were collected, of which 60% and 40% were randomly split into a training set and a testing set, respectively.

3 Methodology

In this paper, first, 20-two CP SAR parameters are

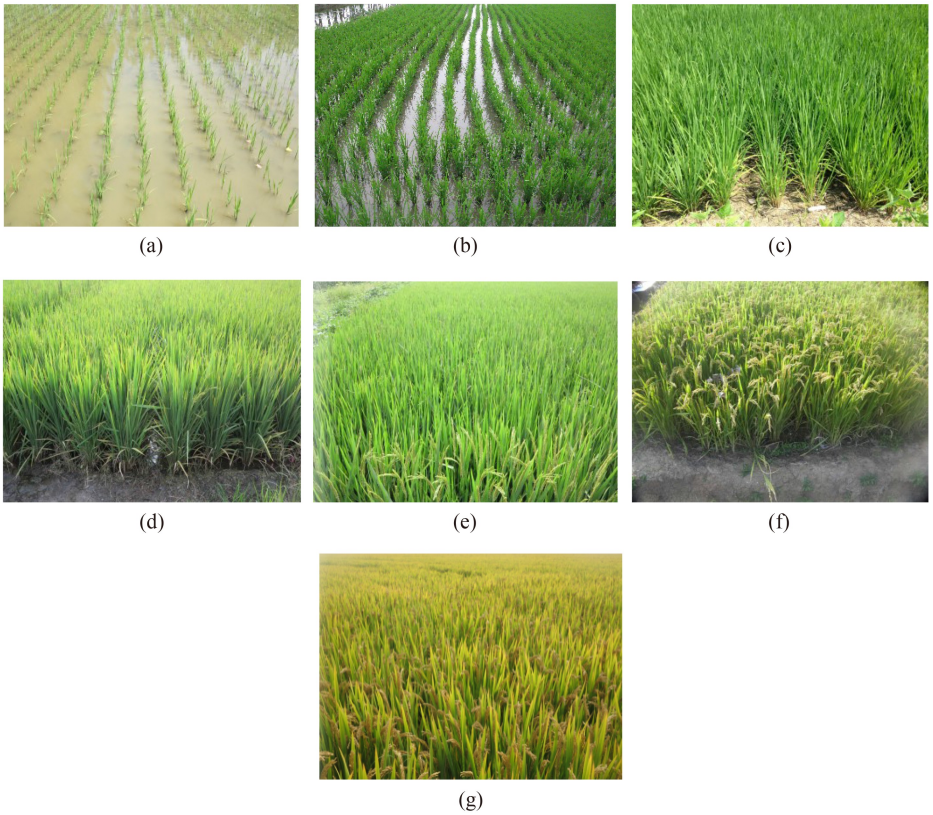

Fig. 2 Image of seven phenological periods of rice growth for the T-H rice paddy in the study area. (a) 2012-6-27 seedling stage; (b) 2012-7-11 tillering stage; (c) 2012-7-21 elongation stage; (d) 2012-8-4 heading stage; (e) 2012-8-28 flowering stage; (f) 2012-9-21 milk stage; (g) 2012-10-15 dough stage.

Table 1 Full-polarization SAR data parameters of multitemporal RADARSAT-2

Number (*i*)	Data acquisition date (D/M/Y)	DoY (Day of Year)	Image mode	Pixel Spacing (A × R, m)	Incidence Angle/(°)	Product
1	27 June 2012	179	FQ20W[1)]	5.2 × 7.6	38–41	SLC[2)]
2	11 July 2012	193	FQ9W	5.2 × 7.6	27–30	SLC
3	21 July 2012	203	FQ20W	5.2 × 7.6	38–41	SLC
4	4 August 2012	217	FQ9W	5.2 × 7.6	27–30	SLC
5	28 August 2012	241	FQ9W	5.2 × 7.6	27–30	SLC
6	21 September 2012	265	FQ9W	5.2 × 7.6	27–30	SLC
7	15 October 2012	289	FQ9W	5.2 × 7.6	27–30	SLC

Notes: 1) FQW = fine quad-polarimetry wide, 20 or 9 is the number of beam positions, which is related to the incidence angle; 2) SLC = single look complex.

simulated and extracted from seven temporal full-polarization SAR data sets, and the parameters ΔCP_{DoY} are calculated. Second, six machine learning methods were employed to carry out fine classification of rice paddies, and the accuracy of the classification results was verified and evaluated. Figure 3 shows the specific flow chart of the methodology.

3.1 Simulation, extraction and preprocessing of CP SAR data

3.1.1 Data simulation

In this paper, the circular transmit and linear receive (CTLR) mode is used to simulate CP SAR data with the RADARSAT-2 full polarimetric SAR (Raney, 2007). The

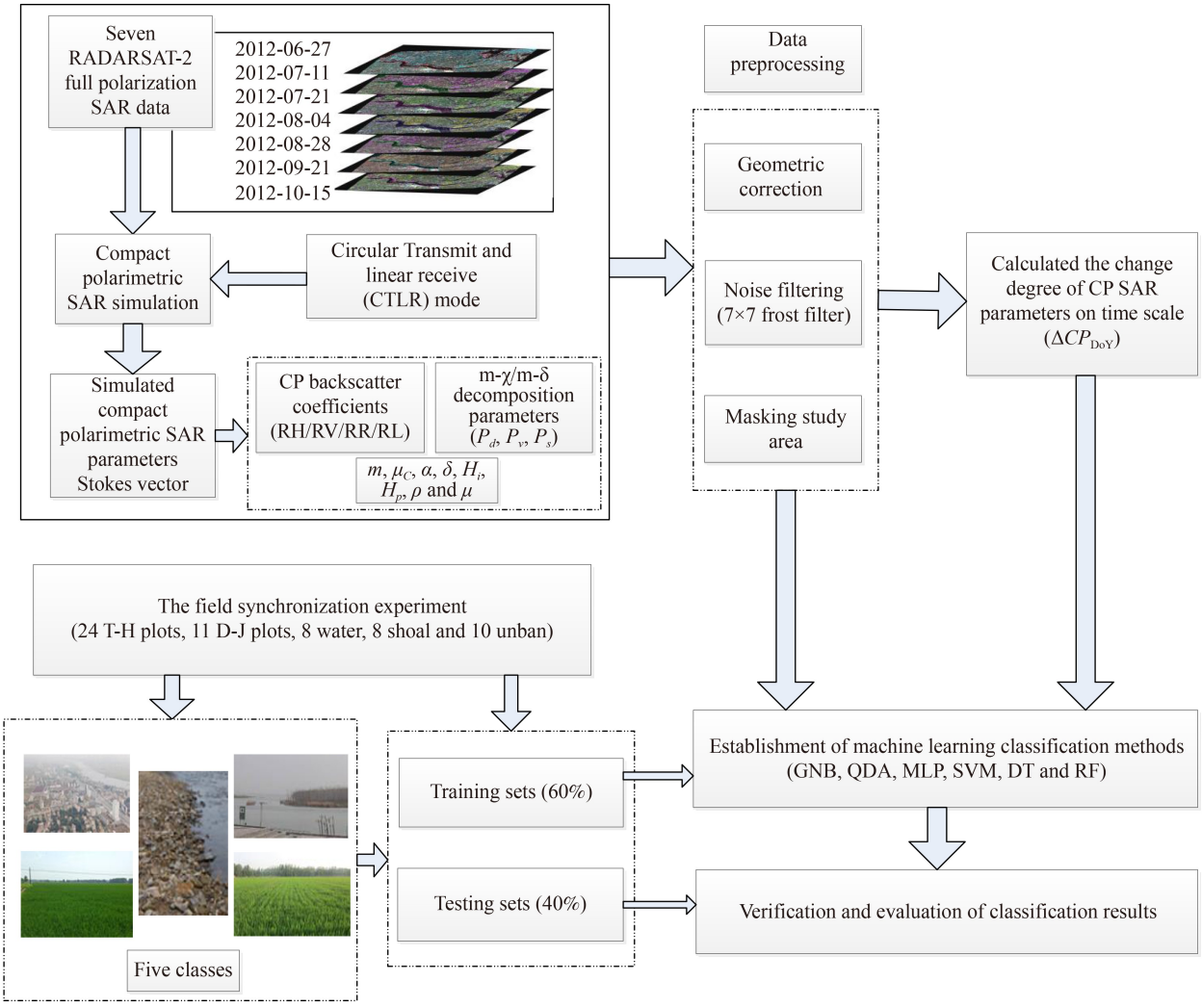

Fig. 3 Specific flow chart of the methodology.

simulation process of CP SAR data can be summarized in 5 steps.

1) Based on the Sinclair matrix of full-polarization SAR data, the electric vector E_B of the target backscattering field is constructed when the sensor emits a right circularly polarized R electromagnetic wave.

2) When the antenna sends and receives a linear polarization (H and V) signal, the E_H and E_V components are calculated (Touzi et al., 2004; Raney, 2007).

3) This step is performed to calculate the four elements of the coherence matrix J.

4) Based on the elements of matrix J, the Stokes vector S is calculated.

5) According to the relation between the Sinclair matrix [I] and the covariance matrix, C_3, we establish a relation between the matrix elements of the full-polarization SAR data and the Stokes vector for the CP SAR.

3.1.2 Parameters extraction

For the simulated CP SAR data, we extracted 20-two characteristic parameters of each temporal CP SAR data, which were divided into 4 backscattering parameters, 4 Stokes parameters, the derived parameters of the Stokes vector, 6 polarization decomposition parameters, and other characterization nonintensity parameters. In addition, the change degree of the CP SAR parameters on a time scale, which is detailed in Section 3.2, was extracted.

Four CP backscattering coefficients were simulated in the right circular transmit and horizontal linear receive (RH), right circular transmit and vertical linear receive (RV), right circular transmit and right circular receive (RR), and right circular transmit and left circular receive (RL) from the full-polarization Stokes vector S. In addition, the relative phase angle δ is obtained from RH and RV polarized scattering echoes. The calculation details are described by Eqs. (1)–(5) as follows:

$$\sigma^0_{\mathrm{RH}} = [1,1,0,0]\times S, \tag{1}$$

$$\sigma^0_{\mathrm{RV}} = [1,-1,0,0]\times S, \tag{2}$$

$$\sigma^0_{\mathrm{RR}} = [1,0,0,-1]\times S, \tag{3}$$

$$\sigma^0_{\mathrm{RL}} = [1,0,0,1]\times S, \tag{4}$$

$$\delta = \tan^{-1}\left(\frac{S_4}{S_3}\right), 0<\delta<\frac{\pi}{2}, \tag{5}$$

where S is the Stokes vector, and S_3 and S_4 are the third component and fourth component, respectively, of the Stokes vector. δ provides the phase information about the scattering target (Raney, 2006).

Four components of the Stokes vector, including S_1, S_2, S_3, and S_4, represent the intensity and polarization state of the radar scattering echo. Among them, S_0 and S_1 are closely related to the total backscattering intensity and contain the main backscattering energy, while S_3 is closely related to ground surface scattering (Raney et al., 2012a).

σ^0_{RH} is more sensitive when the scattering element changes in the horizontal direction, and σ^0_{RV} is more sensitive in the vertical direction, both of which are mainly attributed to the depolarization of volume scattering. σ^0_{RR} is sensitive to double-bounce scattering.

The three scattering components of the m-χ and m-δ decomposition (Raney et al., 2012a, 2012b), the physical meanings of which were similar to that of the Freeman-Durden decomposition for full-polarization SAR, were generated from the simulated CP SAR data (Yin and Yang, 2014).

The derived parameters of the Stokes vector mainly include the polarization degree m, circular polarization ratio μ_{C} and average scattering angle α (Cloude et al., 2012).

The average scattering angle α is related to the scattering mechanism of the target. $\alpha = 0$ corresponds to double-bounce scattering; $\alpha = \pi/4$ corresponds to volume scattering; and $\alpha = \pi/2$ corresponds to surface scattering. The formula is expressed as follows:

$$\alpha = \frac{1}{2}\tan^{-1}\left(\left(S_2^2+S_3^2\right)^{\frac{1}{2}}/(\pm S_4)\right), \tag{6}$$

The derived parameter of the Stokes vector, the circular polarization ratio μ_{C}, is defined as the ratio of the difference to the sum of the first and fourth components of the Stokes vector. The formula is expressed as follows:

$$\mu_{\mathrm{C}} = (S_1 - S_4)/(S_1 + S_4), \tag{7}$$

The consistency coefficient μ, whose physical significance is similar to the average scattering angle, is related to the scattering mechanism of the target. t_1 and t_2 are the empirical coefficients of −1 to 1. For $-1 < \mu < t_2$, the scattering components of the target mainly comprise double-bounce scattering. For $t_2 < \mu < t_1$, the scattering components of the target are mainly scattered by volume. For $t_1 < \mu < 1$, the scattering components of the target are mainly reflected by surface (Truong-Loi et al., 2009):

$$\mu = \frac{2Im\left\langle s_{\mathrm{RH}} s^*_{\mathrm{RV}}\right\rangle}{\left\langle s_{\mathrm{RH}} s^*_{\mathrm{RH}}\right\rangle + \left\langle s_{\mathrm{RV}} s^*_{\mathrm{RV}}\right\rangle}. \tag{8}$$

In this paper, ρ represents the correlation of the scattering matrix elements S_{RH} and S_{RV}, which is described by Eq. (9) as follows:

$$\rho = \frac{\sqrt{\left\langle\left|s_{\mathrm{RH}} s^*_{\mathrm{RV}}\right|\right\rangle}}{\sqrt{\left\langle\left|s_{\mathrm{RH}} s^*_{\mathrm{RH}}\right|\right\rangle + \left\langle\left|s_{\mathrm{RV}} s^*_{\mathrm{RV}}\right|\right\rangle}}, \tag{9}$$

Shannon entropy, which contains abundant scattering information of ground objects, is composed of two components. The first component is the intensity component $H_{i,}$ and the second component is the polarimetric component H_p. The Shannon entropy intensity H_i, which represents the strength of the coherence matrix, is derived from the coherence matrix (Réfrégier and Morio, 2006). The Shannon entropy polarimetric component H_p represents the polarization of Bakarat (p_T). The formula is expressed as follows:

$$H_i = 2\lg\left(\frac{\pi\, e\mathrm{Tr}[T_2]}{2}\right), \tag{10}$$

$$H_p = \lg\left(4\frac{\mathrm{Det}[T_2]}{\mathrm{Tr}[T_2]^2}\right), \tag{11}$$

$$p_T = \sqrt{1-4\frac{\mathrm{Det}[T_2]}{\mathrm{Tr}[T_2]^2}}, \tag{12}$$

where T_2 is the coherence matrix, $\mathrm{Tr}[T_2]$ represents the trace of coherence matrix T_2, and $\mathrm{Det}[T_2]$ represents the value of the determinant of coherent matrix T_2.

3.1.3 Preprocessing of CP SAR data

After CP SAR data simulation and parameter extraction, we preprocess the data. The characteristic parameters of CP SAR, such as radiometric calibration, geometric correction, and speckle noise filtering, are preprocessed. In addition, a 7 × 7 frost filter was applied to all the CP SAR parameters. The Frost filter, which is based on the multiplicative noise model, is suitable for coherent speckle filtering and is a Wiener adaptive filter. In addition, the Frost filter can be approximately regarded as a low-pass filter, which can well smooth the speckle noise in the smooth uniform region.

3.2 Defining the change degree of CP SAR parameters on a time scale (ΔCP_{DoY})

There is a large gap in the backscattering amount among urban areas, water areas and rice paddies, and each temporal CP parameter can be clearly distinguished. For shoals, weeds continuously grow over time, and the backscattering of weeds and rice paddies also differs in different time phases. However, for the two types of rice paddies, these backscattering components exhibit minimal difference at the same time phase. Therefore, it is difficult to distinguish the two types of rice paddies using CP SAR parameters. To improve the accuracy of the fine classification of rice paddies, the change degree of CP SAR parameters on a time scale (ΔCP_{DoY}) is considered. The ΔCP_{DoY} is described by Eqs. (13–14) as follows:

$$T_i = \mathrm{DoY}_{i+1} - \mathrm{DoY}_i,\ \ i = 1,2,...,6, \tag{13}$$

$$\Delta \mathrm{CP}_{\mathrm{DoY}} = \left|\mathrm{CP}_{i+1} - CP_i\right| \times \frac{T_i}{2}, \tag{14}$$

where DoY represents Day of Year, i represents the serial number of CP SAR images obtained in chronological order (Table 1), and T_i represents the differential value of DoY. CP_i represents CP parameter values for the i temporal image. $\Delta \mathrm{CP}_{\mathrm{DoY}}$ represents the change degree of CP SAR parameters on a time scale.

Due to the different varieties and sowing methods of rice, the values of $\Delta \mathrm{CP}_{\mathrm{DoY}}$ differ. With the growth of the two types of rice paddies, the scattering values of CP SAR parameters are different, which can provide favorable parameter support for distinguishing and classifying different rice paddies. Therefore, we used $\Delta \mathrm{CP}_{\mathrm{DoY}}$ as a valid parameter to carry out the fine classification of rice paddies. Figure 4 shows a line diagram of $\Delta \mathrm{CP}_{\mathrm{DoY}}$ ($\Delta \mathrm{RH}_{\mathrm{DoY}}$, $\Delta \mathrm{RV}_{\mathrm{DoY}}$, $\Delta \mathrm{RR}_{\mathrm{DoY}}$, and $\Delta \mathrm{RL}_{\mathrm{DoY}}$) for two types of rice paddy classes on a time scale for four polarization modes (RH, RV, RR, and RL).

As shown in Fig. 4, for each polarization mode, there was a great difference between the two types of rice paddies ($\Delta \mathrm{CP}_{\mathrm{DoY}}$). Therefore, we consider $\Delta \mathrm{CP}_{\mathrm{DoY}}$ as favorable characteristic parameters that can improve the accuracy of the classification results by using machine learning methods. In the early growth stage of rice, because the underlying surface of T-H is water and the underlying surface of D-J is soil, the rice paddy of T-H is prone to surface scattering. Therefore, the values of $\Delta \mathrm{RH}_{\mathrm{DoY}}$, $\Delta \mathrm{RV}_{\mathrm{DoY}}$, $\Delta \mathrm{RR}_{\mathrm{DoY}}$, and $\Delta \mathrm{RL}_{\mathrm{DoY}}$ of D-J are obviously larger than those of T-H. With the continuous growth of the plant body of rice, the plant body of D-J has the characteristics of thick stalks, rapid growth and higher density. Therefore, the values of $\Delta \mathrm{RH}_{\mathrm{DoY}}$, $\Delta \mathrm{RV}_{\mathrm{DoY}}$, $\Delta \mathrm{RR}_{\mathrm{DoY}}$, $\Delta \mathrm{RR}_{\mathrm{DoY}}$, and $\Delta \mathrm{RL}_{\mathrm{DoY}}$ of D-J are significantly greater than those of T-H in the early stage of rice growth. In the mature stage of the two types of rice, because the growth of the rice body is basically stable, the water and soil of the underlying surface are covered by the plant body of rice, and the difference in the varieties and sowing methods of rice has minimal influence on the scattering value of CP SAR parameters on a time scale.

As a whole, the line diagram of $\Delta \mathrm{RV}_{\mathrm{DoY}}$ has the best effect on distinguishing the two types of rice paddies, and the difference in the scattering value between the two types of rice paddies is the largest.

The reason for these findings is that backscattering of the RV mainly represents the depolarization of volume scattering and is more sensitive when the scattering element changes in the vertical direction. The differences between the two types of rice paddies are mainly reflected in the variation in body scattering. In addition, D-J is stronger and grows faster than T-H, so the change in the scattering value is large in the vertical direction for the two rice paddy fields.

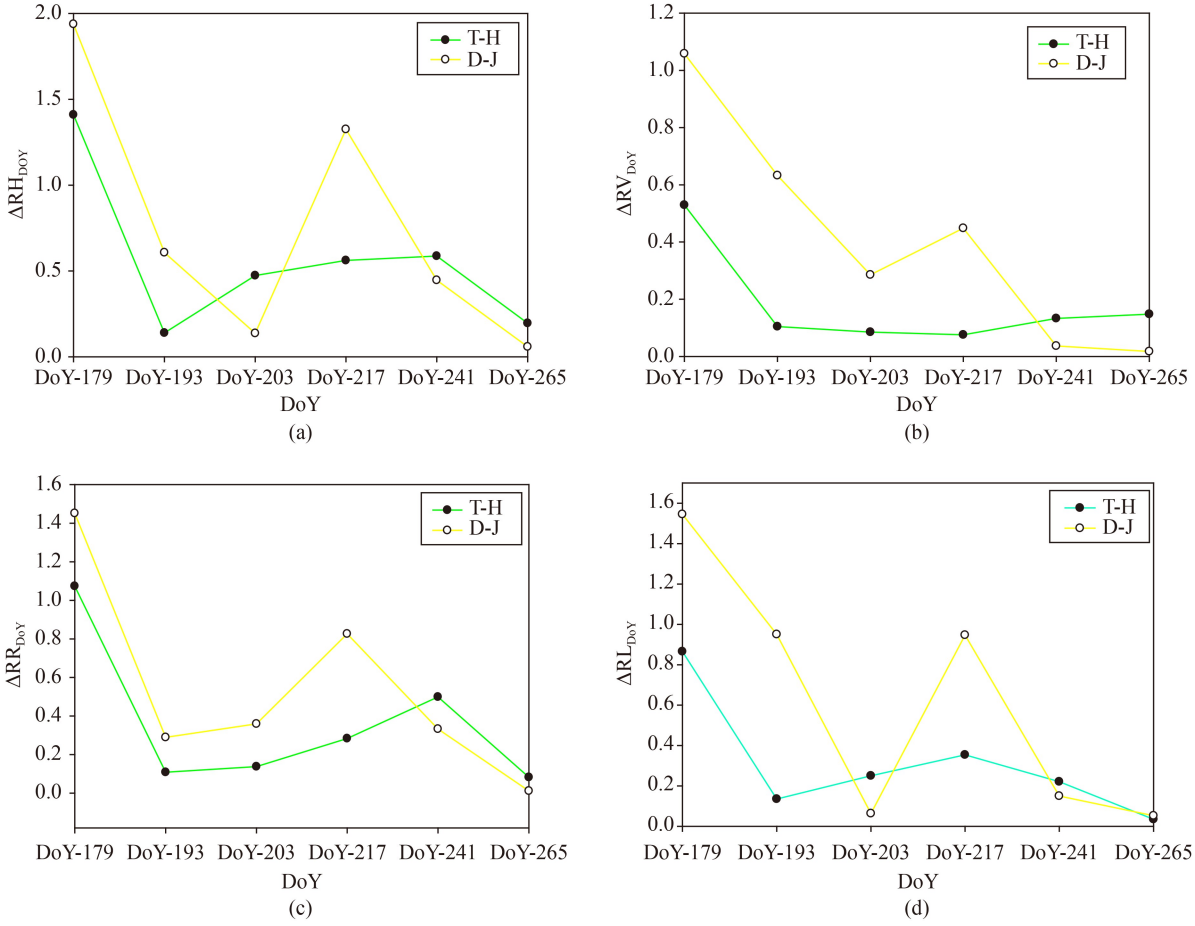

Fig. 4 Line diagram of ΔCP_{DoY} ((a) ΔRH_{DoY}, (b) ΔRV_{DoY}, (c) ΔRR_{DoY}, and (d) ΔRL_{DoY}) for two types of rice classes on a time scale for four polarization modes (RH, RV, RR, and RL).

3.3 Six classification methods of machine learning

Six machine learning models, i.e., Gaussian naive Bayes (GNB), quadratic discriminant analysis (QDA), multilayer perceptron (MLP), SVM, DT, and RF, were selected to identify surface features.

Naive Bayes (NB) is based on the Bayes theorem with the "naive" hypothesis of conditional independence (Bressan and Vitria, 2002; Harzevili and Alizadeh, 2021). GNB is the extension of NB that follows a Gaussian normal distribution (Pérez et al., 2009; Schlechtriemen et al., 2014; Wang et al., 2016). GNB classifiers still tend to perform very well under unrealistic assumptions. QDA is a variant of linear discriminant analysis (LDA), in which a single covariance matrix is estimated for each type of observation (Zhang, 1997; Li et al., 2012b). QDA is particularly useful if it is known in advance that individual categories exhibit different covariances. If QDA assumes independence of the features, which means that the covariance matrices are diagonal, the resulting classifier is equivalent to the GNB.

The MLP neural network consists of input, hidden, and output layers and is one of the most widely utilized artificial neural networks (ANNs) (LeCun et al., 2015). The model utilized the rectified linear unit (relu) function as the activation function for the hidden layer in this work (He et al., 2015).

The SVM is a very powerful machine learning algorithm that is utilized in different applications, such as classification analysis, regression analysis, and pattern recognition (Suykens and Vandewalle, 1999; Huang et al., 2012). SVMs are based on statistical learning theory that can be applied to obtain a hyperplane for multidimensional data. The space of the labeled input data set is projected into a high-dimensional feature space to create an optimal separating hyperplane that divides the instances into two sides of the hyperplane with minimum generalization error.

The DT is an effective, nonparametric, supervised learning approach for solving classification problems. The DT can categorize or predict the value of a target variable by learning simple decision rules inferred from the data features (Kohavi and John, 1997; Ho, 1998). While the DT has the advantage of being easy to use, understand, and explain, it has a relatively lower predictive accuracy than machine learning methods with more complex decision boundaries. Because of its high prediction accuracy, the RF model is widely employed in

classification problems. As an averaging ensemble method, the driving principle of the RF model is to independently build several estimators (as many trees as base learners and aggregates) and then to average their predictions (Ho, 1998; Breiman, 2001). Due to the reduced variance, on average, the prediction result of the combined tree is better than that of any of the single base trees.

All the above models were based on the Scikit-Learn machine learning library (Pedregosa et al., 2011) in this paper.

4 Results

Seven temporal CP SAR parameters and ΔCP_{DoY} were utilized to carry out fine classification of rice paddies with six machine learning methods. The classification results were verified; Figure 5 shows the classification results based on six machine learning methods.

4.1 Analysis of classification results

From the six maps of classification results, the water, shoal, and urban areas are clearly distinguished, which is related to the difference in scattering between the three classes of nonrice and two classes of rice paddy. The water area is in the southern river of the study area, and some small ponds in the north-eastern part of the study area are also identified. Shoal is mainly concentrated around rivers and ponds, and the area of this class is the largest on both sides of the river. Buildings are concentrated in the southern part of the study area. Several towns and villages are also identified in the study area. In the south-eastern part of the study area, the rice paddies of T-H, with a uniform distribution, are identified as regular blocks. In the north-western part of the study area, there are no regular blocks in the D-J rice paddy, but they are also identified. The rice in this area is consistent with the direct-sown method.

To better illustrate the advantages and characteristics of machine learning methods in the fine classification of rice paddies, the same area from the six classification maps was selected for a detailed comparative analysis. Figures 6, 7, and 8 show the classification results based on the six machine learning methods in regions 1, 2, and 3, respectively.

Region 1 mainly includes the T-H, D-J, and shoal classes. As shown in Fig. 6, the classification results of the six machine learning methods are essentially consistent in the whole region, with slight differences. For Figs. 6(a), 6(c), and 6(e), the regional classification results of rice paddies are generally consistent. In addition, a small speckle in the left part of the image is also classified as the shoal class. For the results of Figs. 6(b) and 6(d), the QDA and GNB methods are not sensitive to small shoal pieces, and these shoals cannot be identified. For Fig. 6(f), shoal spots exist in the full map distribution, which is obviously impossible for real regional scenes. Therefore, the DT method is too sensitive to identify shoals. In conclusion, the RF, MLP, and SVM methods are better than the QDA, GNB, and DT methods for shoal classification.

Region 2 mainly includes the T-H class, shoals and water, and Region 2 is located in a regular block. Transplanting mode is the main cultivation method of rice in this plot. In addition, there are three small ponds on the right side of this area. For Region 2, the classification results using the six machine learning methods are similar, with slight differences. Six machine learning methods can accurately differentiate T-H rice paddies. In addition, the image on the right side of three small reservoirs was identified, with differences in the areas identified. For the results with the RF, MLP, SVM, and DT methods, the pond water is identified. However, for the QDA and GNB methods, the recognition area of pond water is smaller and that of shoals is larger.

In Region 3, which mainly includes shoal and water classes, shoals are the main class. There are differences among the classification results obtained by different methods. The rectangle block area is a pure shoal in the validation data sets. The RF, MLP, and SVM methods could classify shoals as relatively pure in this area, as shown in Fig. 8. However, some shoals are misclassified as rice paddies because of the different design principles of machine learning methods, especially in Figs. 8(b), 8(d), and 8(f). Selecting Fig. 8(b) as an example, it is known that the covariance of the rice paddy and shoal classes differs. Based on the principle of QDA, rice paddy and shoal can be distinguished. However, in the shoal class, because the covariance of the shoal class in Region 3 may be large and certain shoal features are similar to those of rice paddies, QDA mistakenly classifies a small part of the region into two types of rice paddies.

Overall, there is a minor difference in the classification results of the five types of ground objects by using the six machine learning methods, especially for the two types of rice paddies. However, the RF, MLP, and SVM methods are better than QDA, GNB, and DT in discriminating the shoal class. Among them, the DT method is too sensitive for shoal identification. In addition, a small number of misclassification results for the two types of rice paddies are classified into the relatively pure shoal class with the QDA, GNB, and DT methods.

4.2 Classification accuracy verification

The study area is classified into five classes: T-H, D-J, water, shoal, and urban. When the RADARSAT-2 satellite passes over the study area, the ground vector data are synchronously collected by a GPS. Testing sets are

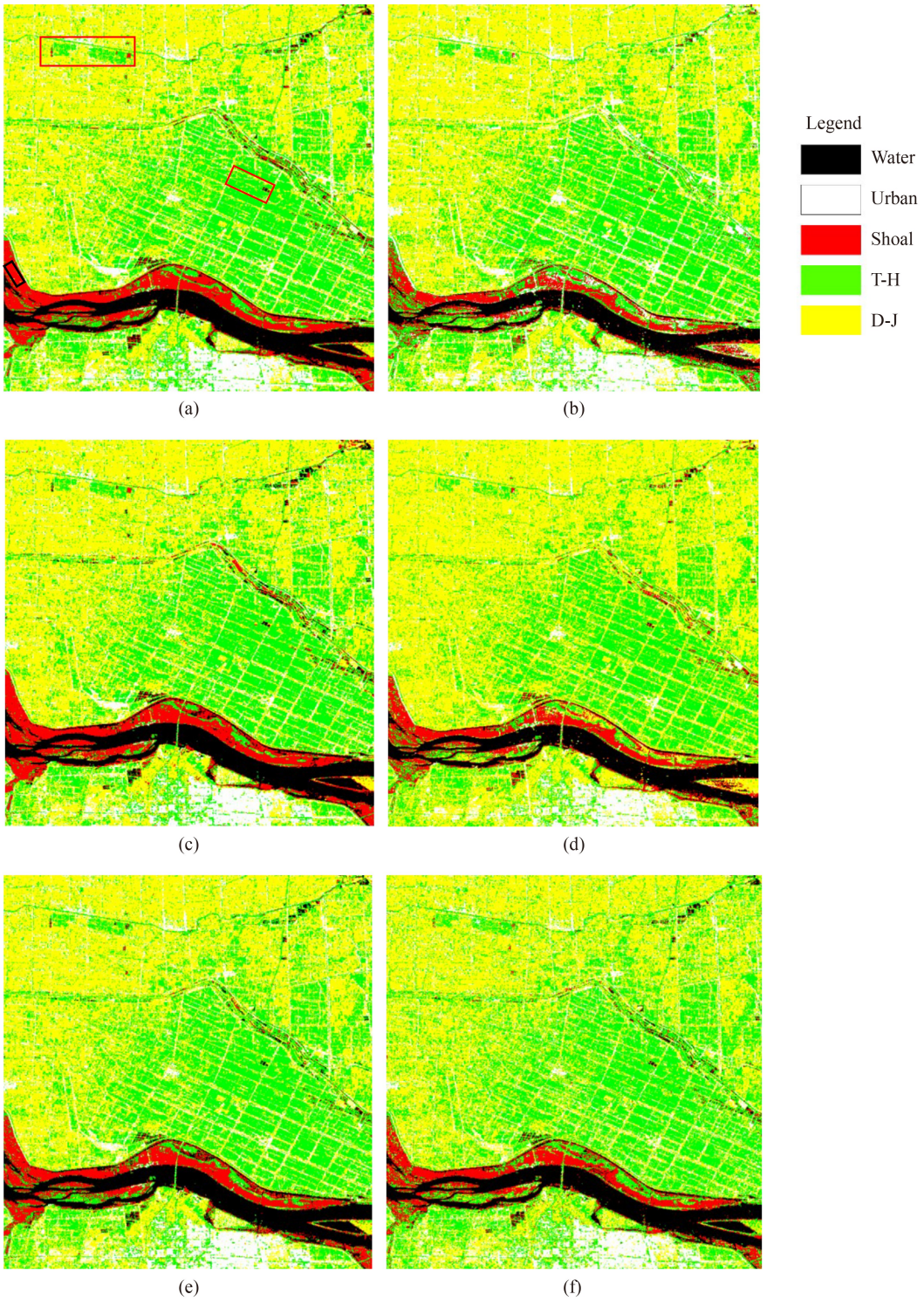

Fig. 5 Classification results based on six machine learning methods. (a) RF; (b) QDA; (c) MLP; (d) GNB; (e) SVM; (f) DT.

used to evaluate the accuracy of the classification results. The corresponding classification accuracy of different methods is shown in Table 2.

As shown in Table 2, the overall accuracy obtained by the six machine learning methods is greater than 95.05%, and the Kappa coefficient is greater than 0.937. Therefore, high-precision classification of paddy fields can be achieved. Compared with the six classification methods, the overall accuracy of the RF, MLP, and SVM methods is greater than 97.15%, and the Kappa coefficient is greater than 0.963, which is better than those of QDA, NB, and DT. The performance of the classification accuracy is consistent with the analysis in Section 4.1. We separately analyze the classification

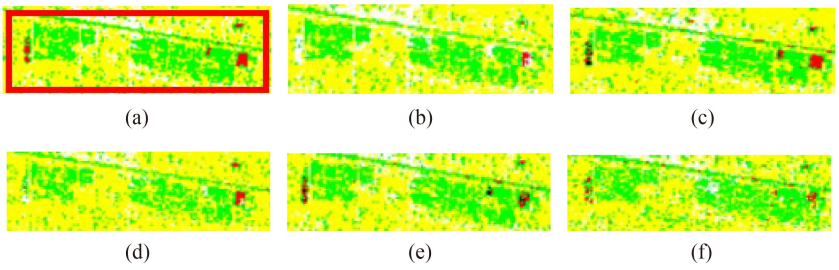

Fig. 6 Classification results based on the six machine learning methods in Region 1. (a) RF; (b) QDA; (c) MLP; (d) GNB; (e) SVM; (f) DT.

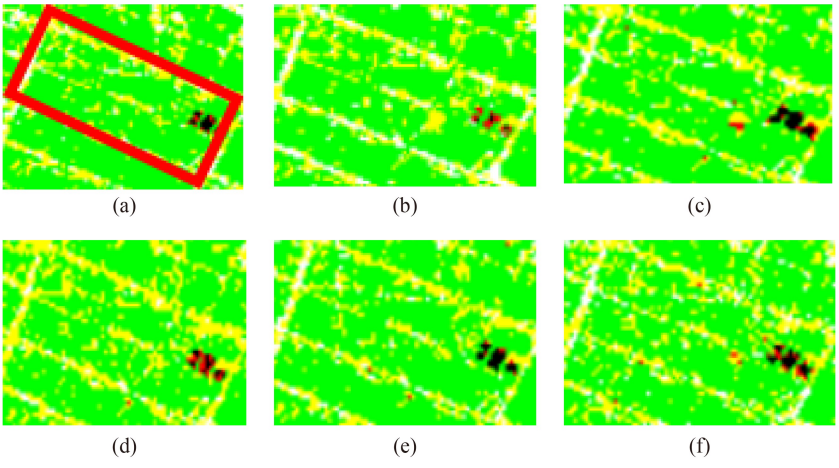

Fig. 7 Same as Fig. 6 but in Region 2. (a) RF; (b) QDA; (c) MLP; (d) GNB; (e) SVM; (f) DT.

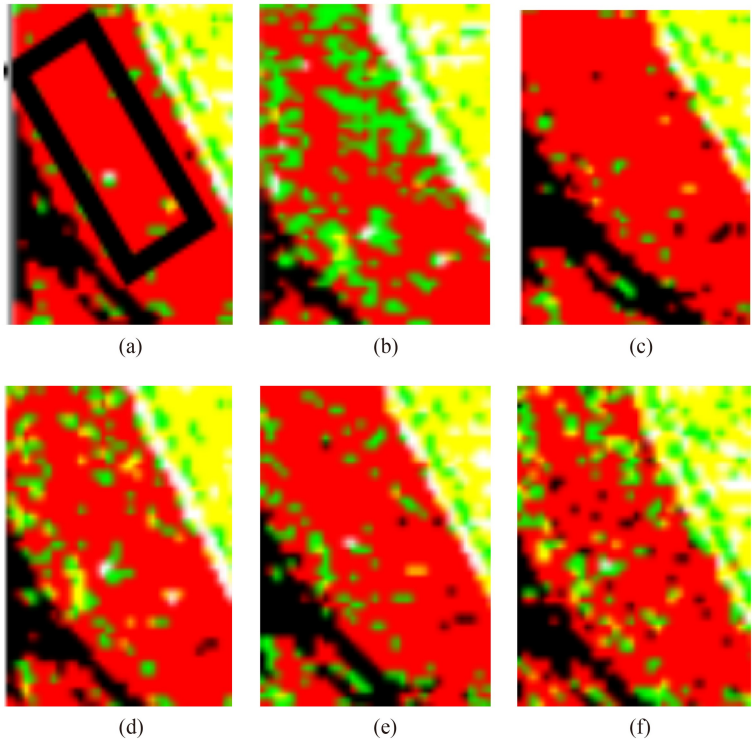

Fig. 8 Same as Fig. 6 but in Region 3. (a) RF; (b) QDA; (c) MLP; (d) GNB; (e) SVM; (f) DT.

accuracy of the five classes. For the average accuracy of T-H, the classification result obtained by the QDA method is the best (> 95.95%). For the average accuracy of D-J, the classification results obtained by the RF and

MLP methods are the best, and the average accuracy of D-J is greater than 96.13%. For the average shoal accuracy, the classification result obtained by the RF method is the best, and the average shoal accuracy is greater than (> 98.34%). For the average accuracy of water, the classification result obtained by the QDA method is the best (> 97.76%). For the average accuracy of urban areas, the six classification methods obtained good classification results (98.00%).

To demonstrate the ability of ΔCP_{DoY} to distinguish between two types of rice paddies, we carried out fine classification of rice paddies by using not only seven temporal CP SAR parameters and ΔCP_{DoY} as features (Fig. 5 and Table 2) but also only the CP parameter as the feature. Compared with only using seven temporal CP SAR parameters for fine classification of rice paddies, our method (seven temporal CP SAR parameters and ΔCP_{DoY} as features) can improve the average accuracy by 1% to 5% for two types of rice paddies.

To better indicate the advantages of this study in the fine classification of rice paddies, Table 3 shows the accuracy table of rice paddy mapping using FP SAR, DP SAR, and CP SAR by certain researchers in recent years. The overall accuracy of the classification results of each study exceeds 89%, which meets the classification requirements. However, most studies only identify one type of rice paddy. In addition, there are few studies on distinguishing different types of rice paddies, and the classification accuracy is not high.

For example, Yang's study was able to distinguish two types of rice paddies, but the user accuracy of the second type of rice paddy was lower (86%). Although Guo's research can distinguish three types of rice paddies, the average accuracy of the third type of rice paddy is only approximately 66%, whose average accuracy is low and cannot well meet the experimental requirements for the third kind of rice paddy. In Wang's research, the classification accuracy of two types of rice paddies reached 91%, and they can achieve precise distinction between two types of rice paddies (Wang et al., 2020). The first type of rice paddy is lodging rice, and the second type of rice paddy is normal rice. The lodging rice suffered from natural disasters and was in an abnormal state, so it failed to distinguish paddy fields with rice classes of different varieties and sowing methods. In comparison (Table 3), the fine classification results for rice paddy in this paper are more accurate by using CP SAR parameters and considering ΔCP_{DoY}. The study results cannot only greatly improve the overall accuracy (more than 95%) but also achieve higher classification accuracy (more than 93%) for the two types of rice paddies than other methods.

Table 2 Accuracy table of classification

Method	Overall Accuracy (OA)/%	Kappa	T-H		D-J		Shoal		Water		Urban	
			UA/%	PA/%	UA/%	PA/%	UA/%	PA/%	UA/%	PA/%	UA/%	PA/%
RF	97.32	0.9656	98.78	88.83	98.48	93.70	97.05	99.64	92.97	99.45	99.81	100.00
QDA	95.92	0.9476	98.92	92.98	97.49	87.65	85.95	98.57	97.42	98.1	98.34	100.00
MLP	97.15	0.9634	98.12	90.12	97.69	94.56	94.75	99.48	94.52	98.98	99.98	98.70
GNB	96.10	0.9499	98.57	84.39	96.25	92.38	92.61	97.98	94.2	99.01	98.68	99.91
SVM	97.37	0.9662	98.14	90.52	98.74	93.12	95.22	99.92	94.28	99.36	99.99	99.77
DT	95.05	0.9365	95.97	85.30	98.50	88.16	89.26	97.98	90.85	98.80	99.28	99.24

Table 3 Accuracy table of rice paddy classification of certain researchers

Study authors	Data type	OA/%	Kappa	Classnumbers	Rice classes	Rice 1		Rice 2		Rice 3	
						UA[3)]/%	PA[4)]/%	UA/%	PA/%	UA/%	PA/%
Guo et al. (2018)	CP SAR	92.57	0.897	5	3	69.57	96.25	88.53	86.39	68.06	45.74
Yang et al. (2014)	CP SAR	93.01	0.932	5	2	94.23	90.61	86.38	95.51	–	–
Brisco et al. (2013)	FP[1)] SAR	–	–	2	1	95	–	–	–	–	–
Uppala et al. (2021)	CP SAR	89.41	0.86	5	1	86.21	89.29	–	–	–	–
Uppala et al. (2015)	CP SAR	90	0.856	5	1	96	100	–	–	–	–
Li (2012a)	FP SAR	91.45	0.85	4	1	92.3	96.51	–	–	–	–
Wang et al. (2020)	DP[2)] SAR andOptical Sensors	91	0.83	2	2	91	91	92	91	–	–
This paper	CP SAR	97.37	0.966	5	2	98.14	90.52	98.74	93.12	–	–

Notes: 1) FP SAR = Full Polarization SAR; 2) DP SAR = Dual Polarization SAR; 3) UA = user accuracy; 4) PA = production accuracy.

5 Discussion

In this paper, based on seven temporal CP SAR data sets of the whole phenological period of rice, we carried out a fine classification experiment of rice paddy. In Section 2, the data that we obtained comprise RADARSAT-2 full polarimetric SAR data. The study area encompasses Jinhu, Jiangsu, China, which contains rice, crab ponds, rivers, urban areas and other ground objects. However, we select one area in the middle of the whole image as an experimental area, accounting for half of the whole image, for two main reasons. The first reason is to remove the interference of buildings, low vegetation and crab ponds. The second reason is that our activity track of the synchronous experiment is mainly carried out in the area that we selected.

In Section 3.1, we tried several filters for multiplicative noise and discovered that the Frost filter has a better filtering effect. Therefore, the Frost filter is adopted. Since the research focus of this paper is the fine classification of rice paddies, we have not conducted additional work on the speckle noise method. In Section 3.2, the main idea of the change degree for CP SAR parameters on a time scale is to consider the CP SAR parameters in the rice growth process over time information, adding the characteristics of two types of rice paddies to promote the classification accuracy. The difference in ΔCP_{DoY} between the two types of rice paddies is shown in Fig. 4. Since we used seven temporal SAR data sets, if more images were obtained during the whole phenological period of rice growth, more parameters representing the characteristics of the two types of rice paddies could be obtained according to the ΔCP_{DoY} formula. In Section 4, we present the results of six machine learning methods based on feature parameters and discuss the classification results in detail. It can be seen that the accuracy of the six classification results is very high due mainly to the following factors. 1) The data collected on the ground have a certain impact on the classification results. When we synchronized the experiment, we basically selected two types of rice paddies with large and regularly shaped plots, which to some extent promoted the accuracy of the classification results. 2) The ground features in the study area exhibit relatively pure classes, and there are almost no other types of ground features, which is also an important aspect. 3) The machine learning methods are suitable for CP SAR data, which also indicates that CP SAR parameters and ΔCP_{DoY} can well characterize the differences between two types of rice paddies and nonrice classes.

In the conclusion, we compare our experimental results with the rice classification results of recent researchers; the comparison reveals that the accuracy of our rice classification is better than that of other methods. Although this finding explains the advantages of this study to some extent, there are still deficiencies in this comparison given the difference in the research areas, data, and satellites utilized by researchers.

In view of the previous discussion, we consider the following points for future work.

1) Although machine learning methods can obtain high accuracy of rice paddy classification, they lack a physical analysis of characteristic parameters on rice classification. Next, we will consider the physical significance of the characteristic parameters. We introduce a feature selection method to extract CP SAR parameters sensitive to distinguishing two types of rice paddies or construct characteristic parameters to improve the classification accuracy.

2) As the study area is unique, we will consider changing the study area to perform rice fine classification experiments in future work so that the experimental results can be fully verified.

6 Conclusions

In this paper, the change degree of CP SAR parameters on a time scale (ΔCP_{DoY}) was first proposed and defined. Based on the multidimensional information and time scale variation of CP SAR parameters, we utilized six machine learning methods to carry out the classification experiments. High-precision results can be obtained with an overall accuracy greater than 95.05% and a Kappa coefficient greater than 0.937. A comparison of the fine classification results of rice paddies with those of recent researchers reveals that our results can improve the overall accuracy by more than 4% and the Kappa coefficient by more than 0.04%. In addition, the RF and SVM methods achieve the best results, with the overall accuracy reaching 97.32% and 97.37% and the Kappa coefficient reaching 0.965 and 0.966, respectively. The average accuracy of the T-H rice paddy is greater than 90.64%. The average accuracy of the D-J rice paddy is greater than 92.57%. Furthermore, we determined that the QDA and GNB methods have low recognition ability for small shoal classes. In addition, the DT classification method is too sensitive for shoal class recognition, which creates a misclassification phenomenon.

This study defined the change degree of CP SAR parameters on a time scale and fully utilized the multidimensional information of CP SAR data. This study improved the accuracy of the fine classification of rice paddies and explored the advantages and disadvantages of six machine methods in rice classification. Based on the research content of this paper, we obtained the high-precision results of the fine classification of rice paddies, which can promote the regional management and rice yield estimation of large-scale and multitype rice in agriculture-related sectors.

Acknowledgments This work was funded in part by the National Natural Science Foundation of China (Grant No. 41871272).

References

Abubakar G A, Wang K, Shahtahamssebi A, Xue X, Belete M, Gudo A J A, Mohamed Shuka K A, Gan M (2020). Mapping maize fields by using multi-temporal Sentinel-1A and Sentinel-2A images in Makarfi, Northern Nigeria, Africa. Sustainability (Basel), 12(6): 2539

Betbeder J, Rapinel S, Corpetti T, Pottier E, Corgne S, Hubert-Moy L (2013). Multi-temporal classification of TerraSAR-X data for wetland vegetation mapping. In: Remote Sensing for Agriculture, Ecosystems, and Hydrology XV part of the 20th International Symposium on Remote Sensing, Dresden, Germany, 2013 Sep 23–26

Bouvet A, Le Toan T, Lam-Dao N (2009). Monitoring of the rice cropping system in the Mekong Delta using ENVISAT/ASAR dual polarization data. IEEE Trans Geosci Remote Sens, 47(2): 517–526

Breiman L (2001). Random forests. Mach Learn, 45(1): 5–32

Bressan M, Vitria J (2002). Improving naive Bayes using class-conditional ICA. In: Garijo F J, Riquelme J C, Toro M, eds. Advances in Artificial Intelligence - Iberamia 2002

Brisco B, Li K, Tedford B, Charbonneau F, Yun S, Murnaghan K (2013). Compact polarimetry assessment for rice and wetland mapping. Int J Remote Sens, 34(6): 1949–1964

Chen H, Li H (2008). Rice recognition using multi-temporal and dual polarized synthetic aperture radar images. In: International Colloquium on Computing, Communication, Control and Management, Guangzhou, China, 2008 Aug 04–05

Cloude S R, Goodenough D G, Chen H (2012). Compact decomposition theory. IEEE Geosci Remote Sens Lett, 9(1): 28–32

de Castro Filho H C, de Carvalho O A Junior, Ferreira de Carvalho O L, de Bem P P, de Moura R S, de Albuquerque A O, Silva C R, Guimaraes Ferreira P H, Guimaraes R F, Trancoso Gomes R A (2020). Rice crop detection using LSTM, Bi-LSTM, and machine learning models from Sentinel-1 time series. Remote Sens (Basel), 12(16): 2655

Dusseux P, Corpetti T, Hubert-Moy L, Corgne S (2014). Combined use of multi-temporal optical and radar satellite images for grassland monitoring. Remote Sens (Basel), 6(7): 6163–6182

Gašparović M, Dobrinic D (2021). Green infrastructure mapping in urban areas using Sentinel-1 imagery. Croat J For Eng, 42(2): 337–356

Guo X, Li K, Wang Z, Li H, Yang Z (2018). Fine classification of rice with multi-temporal compact polarimetric SAR based on SVM + SFS strategy. Remote Sens Land Resour, 30(4): 20

Harzevili N S, Alizadeh S H (2021). Analysis and modeling conditional mutual dependency of metrics in software defect prediction using latent variables. Neurocomputing, 460: 309–330

He K, Zhang X, Ren S, Sun J (2015). Delving deep into rectifiers: surpassing human-level performance on ImageNet classification. In: IEEE International Conference on Computer Vision, Santiago, CHILE, 2015 Dec 11–18

Ho T K (1998). The random subspace method for constructing decision forests. IEEE Trans Pattern Anal Mach Intell, 20(8): 832–844

Huang G B, Zhou H, Ding X, Zhang R (2012). Extreme learning machine for regression and multiclass classification. IEEE Trans Syst Man Cybern B Cybern, 42(2): 513–529

Inoue Y, Sakaiya E (2013). Relationship between X-band backscattering coefficients from high-resolution satellite SAR and biophysical variables in paddy rice. Remote Sens Lett, 4(3): 288–295

Kohavi R, John G H (1997). Wrappers for feature subset selection. Artif Intell, 97(1–2): 273–324

Kucuk C, Taskin G, Erten E (2016). Paddy-rice phenology classification based on machine-learning methods using multitemporal Co-Polar X-Band SAR images. IEEE J Sel Top Appl Earth Obs Remote Sens, 9(6): 2509–2519

Kurosu T, Fujita M, Chiba K (1995). Monitoring of rice crop growth from space using the ERS-1 C-Band SAR. IEEE Trans Geosci Remote Sens, 33(4): 1092–1096

Lardeux C, Frison P L, Tison C, Souyris J C, Stoll B, Fruneau B, Rudant J P (2009). Support vector machine for multifrequency SAR polarimetric data classification. IEEE Trans Geosci Remote Sens, 47(12): 4143–4152

Lardeux C, Frison P L, Tison C, Souyris J C, Stoll B, Fruneau B, Rudant J P (2011). Classification of tropical vegetation using multifrequency partial SAR polarimetry. IEEE Geosci Remote Sens Lett, 8(1): 133–137

LeCun Y, Bengio Y, Hinton G (2015). Deep learning. Nature, 521(7553): 436–444

Le Toan T, Laur H, Mougin E, Lopes A (1989). Multitemporal and dual-polarization observations of agricultural vegetation covers by X-Band SAR images. IEEE Trans Geosci Remote Sens, 27(6): 709–718

Le Toan T, Ribbes F, Wang L F, Floury N, Ding K H, Kong J A, Fujita M, Kurosu T (1997). Rice crop mapping and monitoring using ERS-1 data based on experiment and modeling results. IEEE Trans Geosci Remote Sens, 35(1): 41–56

Li K, Zhang F, Shao Y, Cai A, Yuan J, Touzi R (2011). Polarization signature analysis of paddy rice in southern China. Can J Rem Sens, 37(1): 122–135

Li K, Brisco B, Yun S, Touzi R (2012a). Polarimetric decomposition with RADARSAT-2 for rice mapping and monitoring. Can J Rem Sens, 38(2): 169–179

Li W, Prasad S, Fowler J E, Bruce L M (2012b). Locality-preserving dimensionality reduction and classification for hyperspectral image analysis. IEEE Trans Geosci Remote Sens, 50(4): 1185–1198

Ndikumana E, Ho Tong Minh D, Baghdadi N, Courault D, Hossard L (2018). Deep recurrent neural network for agricultural classification using multitemporal SAR Sentinel-1 for Camargue, France. Remote Sens (Basel), 10(8): 1217

Onojeghuo A O, Blackburn G A, Wang Q, Atkinson P M, Kindred D, Miao Y (2018). Mapping paddy rice fields by applying machine learning algorithms to multi-temporal Sentinel-1A and Landsat data. Int J Remote Sens, 39(4): 1042–1067

Park S, Im J, Park S, Yoo C, Han H, Rhee J (2018). Classification and mapping of paddy rice by combining Landsat and SAR time series data. Remote Sens (Basel), 10(3): 447

Pedregosa F, Varoquaux G, Gramfort A, Michel V, Thirion B, Grisel O, Blondel M, Prettenhofer P, Weiss R, Dubourg V, Vanderplas J, Passos A, Cournapeau D, Brucher M, Perrot M, Duchesnay E (2011). Scikit-learn: machine learning in python. J Mach Learn Res, 12: 2825

Pérez A, Larranaga P, Inza I (2009). Bayesian classifiers based on kernel density estimation: flexible classifiers. Int J Approx Reason, 50(2): 341–362

Raney R K (2006). Dual-polarized SAR and Stokes parameters. IEEE Geosci Remote Sens Lett, 3(3): 317–319

Raney R K (2007). Hybrid-polarity SAR architecture. IEEE Trans Geosci Remote Sens, 45(11): 3397–3404

Raney R K, Cahill J T S, Patterson G W, Bussey D B J (2012a). The m-chi decomposition of hybrid dual-polarimetric radar data with application to lunar craters. J Geophys Res, 117(E12): E00H21

Raney R K, Cahill J T S, Patterson G W, Bussey D B J (2012b). The m-chi decomposition of hybrid dual-polarimetric radar data. In: IEEE International Geoscience and Remote Sensing Symposium (IGARSS), Munich, GERMANY, 2012 Jul 22–27

Ranjan A K, Parida B R (2019). Paddy acreage mapping and yield prediction using sentinel-based optical and SAR data in Sahibganj District, Jharkhand (India). Spatial Inform Res, 27(4): 399–410

Réfrégier P, Morio J (2006). Shannon entropy of partially polarized and partially coherent light with Gaussian fluctuations. J Opt Soc Am A Opt Image Sci Vis, 23(12): 3036–3044

Schlechtriemen J, Wedel A, Hillenbrand J, Breuel G, Kuhnert K-D (2014). A lane change detection approach using feature ranking with maximized predictive power. In: IEEE Intelligent Vehicles Symposium (IV), Dearborn, MI, 2014 Jun 08–11

Shao Y, Fan X T, Liu H, Xiao J H, Ross S, Brisco B, Brown R, Staples G (2001). Rice monitoring and production estimation using multitemporal RADARSAT. Remote Sens Environ, 76(3): 310–325

Suykens J A K, Vandewalle J (1999). Least squares support vector machine classifiers. Neural Process Lett, 9(3): 293–300

Thorp K R, Drajat D (2021). Deep machine learning with Sentinel satellite data to map paddy rice production stages across West Java, Indonesia. Remote Sens Environ, 265: 112679

Touzi R, Boerner W M, Lee J S, Lueneburg E (2004). A review of polarimetry in the context of synthetic aperture radar: concepts and information extraction. Can J Rem Sens, 30(3): 380–407

Truong-Loi M L, Freeman A, Dubois-Fernandez P C, Pottier E (2009). Estimation of soil moisture and faraday rotation from bare surfaces using compact polarimetry. IEEE Trans Geosci Remote Sens, 47(11): 3608–3615

Uppala D, Kothapalli R V, Poloju S, Mullapudi S S V R, Dadhwal V K (2015). Rice crop discrimination using single date RISAT1 hybrid (RH, RV) polarimetric data. Photogramm Eng Remote Sensing, 81(7): 557–563

Uppala D, Somepalli V, Venkata R K, Rama S M V (2021). Identification of optimal single date for rice crop discrimination and relationships between backscatter and biophysical parameters using RISAT-1 hybrid polarimetric SAR data. Geocarto Int, 36(17): 2010–2022

van Beijma S, Comber A, Lamb A (2014). Random forest classification of salt marsh vegetation habitats using quad-polarimetric airborne SAR, elevation and optical RS data. Remote Sens Environ, 149: 118–129

Wang J, Li K, Shao Y, Zhang F, Wang Z, Guo X, Qin Y, Liu X (2020). Analysis of combining SAR and optical optimal parameters to classify typhoon-invasion lodged rice: a case study using the random forest method. Sensors (Basel), 20(24): 7346

Wang S, Gao R, Wang L (2016). Bayesian network classifiers based on Gaussian kernel density. Expert Syst Appl, 51: 207–217

Waske B, Braun M (2009). Classifier ensembles for land cover mapping using multitemporal SAR imagery. ISPRS J Photogramm Remote Sens, 64(5): 450–457

Yang Z, Li K, Liu L, Shao Y, Brisco B, Li W (2014). Rice growth monitoring using simulated compact polarimetric C band SAR. Radio Sci, 49(12): 1300–1315

Yin J, Yang J (2014). Ship detection by using the m-chi and m-delta decompositions. In: IEEE International Geoscience and Remote Sensing Symposium (IGARSS), Quebec City, Canada, 2014 Jul 13–18

Yu Y, Li M, Fu Y (2018). Forest type identification by random forest classification combined with SPOT and multitemporal SAR data. J For Res, 29(5): 1407–1414

Zhang M Q (1997). Identification of protein coding regions in the human genome by quadratic discriminant analysis. Proc Natl Acad Sci USA, 94(2): 565–568

Zhang X, Xu J, Chen Y, Xu K, Wang D (2021). Coastal wetland classification with GF-3 polarimetric SAR imagery by using object-oriented random forest algorithm. Sensors (Basel), 21(10): 3395